AIChE

Design of a Model-Based Feedback Controller for Active Sorting and Synchronization of Droplets in a Microfluidic Loop

Jeevan Maddala, Babji Srinivasan, Swastika S. Bithi, Siva A. Vanapalli, and Raghunathan Rengaswamy
Dept. of Chemical Engineering, Texas Tech University, Lubbock, TX 79409

DOI 10.1002/aic.12740
Published online August 23, 2011 in Wiley Online Library (wileyonlinelibrary.com).

The transport of confined droplets in fluidic networks can lead to complex spatiotemporal dynamics, precluding full control of the position of droplets in the network. Here, we report the design of a model-based feedback controller that can actively regulate droplet positions in a network. We specifically consider droplet dynamics in a microfluidic loop where a main channel splits into two and recombines. Consistent with previous studies, we find that without active control, the dynamics of droplets in the loop can range from periodic to chaotic behaviors. However, by implementing the model-based feedback controller, we show that the droplets can be made to sort alternately into the branches of the loop as well as to synchronize the times at which pairs of droplets exit the loop. In particular, our computations demonstrate that the controller is capable of executing remarkable droplet sort-synchronization tasks in the otherwise chaotic dynamics in the loop. The design of our controller incorporates a hydrodynamic network model, that is, capable of predicting droplet positions and subsequently delivering an actuation to the branches in the loop through elastomeric valves. Efficacy of the controller is discussed in terms of actuation characteristics and constraints imposed by elastomeric valves. The model-based feedback controller framework presented in this study is likely to promote the development of lab-on-chip technologies in which droplet manipulation tasks are executed with active control. © 2011 American Institute of Chemical Engineers *AIChE J,* 58: 2120–2130, 2012

Keywords: microfluidics, control, loop dynamics, network model, elastomeric membrane valves

Introduction

Droplet-based microfluidics is the cornerstone of many lab-on-chip technologies. Several reports exists on the use of microfluidic droplets as microreactors for applications in protein crystallization,[1] integration and automation of biochemical assays,[2] high throughput screening of cells,[3] fabrication of micro and nano particles,[4–7] and single cell analysis.[8] In these applications, the microfluidic devices are often limited to being droplet generators. To handle the complexity of biological analysis, there is a need to incorporate additional tasks such as droplet sorting,[9] synchronization,[10] merging[11,12] and storing[13–18] in these devices. One attractive approach of designing such integrated devices would be to transport confined droplets through cleverly engineered fluidic networks where these tasks can be accomplished passively. Although few studies have shown progress in this direction[10,9,19–22] recent works have highlighted that the spatiotemporal dynamics of droplets in fluidic networks as simple as a loop (where a main channel splits into two and recombines) can be quite complex, ranging from periodic to chaotic behaviors.[23–28] The decision making of the droplets at the bifurcations together with hydrodynamic resistive interactions were considered to be the source of such nonlinear effects. Given these nonlinear effects, implementing droplet manipulation tasks such as sorting and merging in fluidic networks can be quite challenging. As a result studies have resorted to manipulating droplets actively in devices using electric fields[29–35] and elastomeric membrane valve actuation.[36]

In this work, we introduce a framework for designing a model-based feedback controller that actively manipulates droplet positions in a microfluidic network. To demonstrate the power of the model-based feedback controller approach, we consider a scenario shown in Figure 1, where a microfluidic train of alternating black and white droplets enters the loop at a fixed frequency, and the black (B) and white (W) drops need to be sorted into the lower and upper branches, respectively. Furthermore the residence times of the drops in the branches need to be synchronized so that they have the possibility to merge at the exit of the loop. Note that although we specifically consider merging *here*, our approach is capable of handling other synchronization constraints, *e.g.*, achieving a constant delay between drops at the exit. Because of the non-linear droplet dynamics in the loop, it is evident that accomplishing these sort-synchronization objectives passively in the loop is extremely difficult. One possible strategy for achieving these objectives actively is illustrated in Figure 1. It involves integration of single-layer elastomeric membrane valves[37] in the vicinity of the branches, so that they can be actuated to modulate the hydrodynamic resistances of the branches and correspondingly the droplet positions. In addition, a controller is incorporated that reads-in the instantaneous positions of the

Correspondence concerning this article should be addressed to S. A. Vanapalli at siva.vanapalli@ttu.edu or R. Rengaswamy at raghu.rengasamy@ttu.edu.

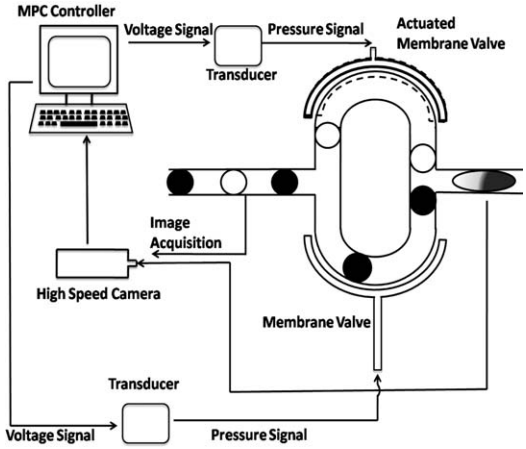

Figure 1. A possible online implementation scheme to sort alternate black and white droplets into upper and lower branches and synchronize them at the exit of the loop device.

droplets through image analysis and subsequently delivers a control action to the valve to modulate the hydrodynamic resistance in the branch. The focus of this study is to design this controller by pursuing the following two aims. First, it is evident that a model needs to be incorporated into the controller, so that future control moves can be estimated from current droplet positions. In this regard, we assess if a recently proposed network model[24] for understanding nonlinear dynamics of droplets can be utilized in the design of the controller. We do so by considering specific cases of experimentally observed nonlinear dynamics of droplets in a loop and determining whether the network model can reproduce these experimental cases. Second, given realistic bounds on the variation in the hydrodynamic resistance of the branches due to valve actuation, we assess if operating envelopes exist for specific cases of nonlinear dynamics that lead to successful sorting and synchronization of droplets.

Experimental Assessment of the Network Model

In this section, experiments that were performed to assess the network model along with its description is discussed. The loop device shown in Figure 2a was fabricated using soft lithography and is similar to that discussed by Fuerstman et al.[23] The lengths of the upper and lower branches were measured to be 2237 μm and 2217 μm. The width and the height of the channels were measured using a scanning electron microscope and are 50 μm and 100 μm, respectively. The aqueous droplets were produced by incorporating a T-junction at the upstream of the loop. Hexadecane (viscosity is 0.003 Pas, density is 773 kg/m^3, Sigma Aldrich) with 2 wt % Span 80 is used as the continuous phase, and a mixture of deionized water and black ink (10: 1 vol/vol) as the dispersed phase. Both phases were driven using syringe pumps (Harvard apparatus, PHD 2000). The fluidic device was mounted on a stereomicroscope stage (Stemi 2000 C). Image acquisition was performed in bright field mode using a CMOS camera (1200.s, PCO, Germany) at 1000 frames per second. The acquired images were analyzed for droplet entry and exit times using a custom code written in MATLAB. Figure 2 illustrates a representative case of the droplet dynamics observed in the loop. A snapshot of the spatiotemporal dynamics of droplets in the loop is shown in Figure 2a, along with the "In" and "Out" windows at which droplet entry and exit times were measured. In Figure 2b, we show that consistent with previous studies[23] droplets enter at nearly regular intervals and exit at intervals that are nonlinearly transformed. We quantify this dynamics using Poincaré s maps for the inputs and outputs as shown in Figure 2c. In here ΔT_n is the (entry or exit) time difference between two successive (nth and $(n-1)$th) droplets and $\langle \Delta T \rangle$ is the mean of the difference in time intervals. All the data collapsing to a single point, i.e., (1,1), in the Poincaré map would imply that the droplets arrive at exactly the same time intervals. We find that a single cluster is associated with the Poincaré map at the "In" window, indicating that droplets enter the loop at a nearly fixed frequency. In contrast, at the "Out" window we find two clusters of data in the Poincaré map, indicating that the droplets exit the loop at two nearly regular intervals. We refer to this behavior as the two period behavior. Similarly three clusters at the outlet will be referred to as three period behavior and if there are no identifiable clusters then we ascribe that behavior as aperiodic.

To assess the model validity for designing the controller, two distinct dynamics of the loop were identified experimentally by varying the oil flow rate at a fixed aqueous flow rate (25 μl/h). We obtained three period and aperiodic cases when the oil flow rates were 450 μl/h and 175 μl/h, respectively. The data obtained from these experiments were

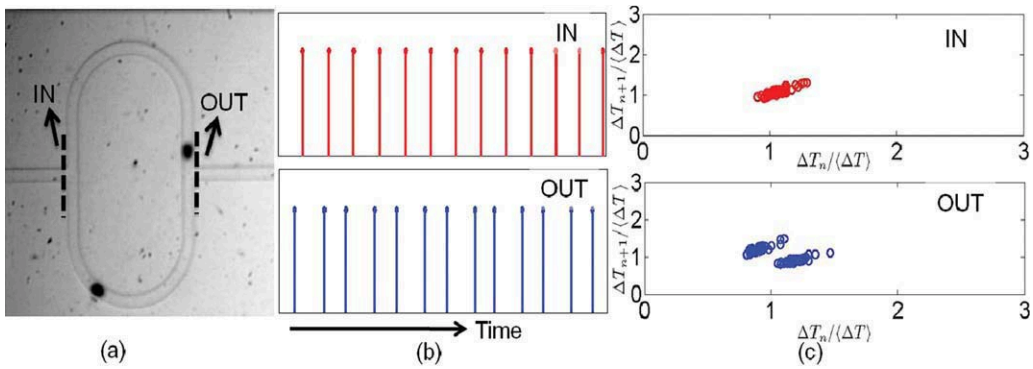

Figure 2. (a) The location of the "In" and "Out" windows in a symmetric microfluidic loop, (b) The time sequence at which droplets are entering and exiting the loop, and (c) The corresponding Poincaré maps, the dynamics are plotted for oil flow rate 750 μl/h and ink flow rate of 25 μl/h.

[Color figure can be viewed in the online issue, which is available at wileyonlinelibrary.com.]

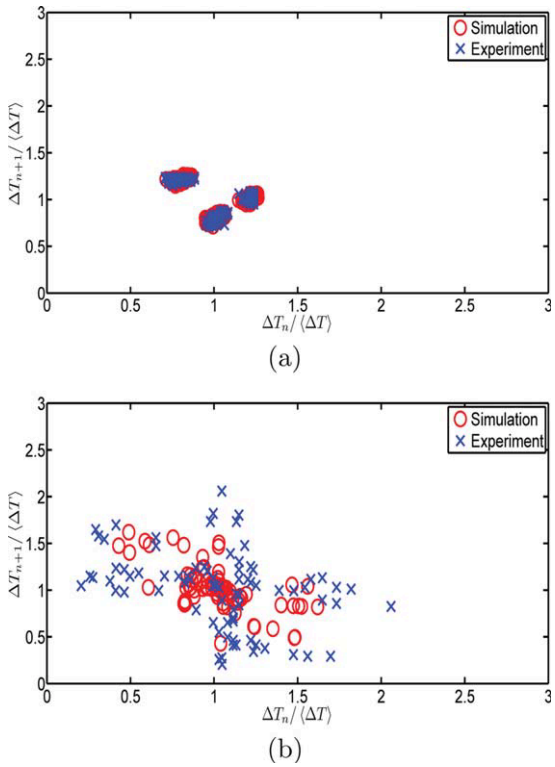

Figure 3. Poincaré maps of (a) three period (b) aperiodic loop dynamics obtained by experiments and simulations; Simulations are done with R_d equal to 1.05 and 4.7 kg/mm^{4}S, respectively and β equal to 1.4 for both the cases.

[Color figure can be viewed in the online issue, which is available at wileyonlinelibrary.com.]

modeled using the network model proposed by Schindler et al.[24] We present a brief overview of the network model for a loop. Flow is conserved at the junction, i.e., net inflow is equal to the outflow which is given by

$$Q_I = Q_U + Q_L \tag{1}$$

where Q_I, Q_U, and Q_L are the flow rates at the inlet, upper, and lower branches, respectively. Analogous to the ohm's law, the pressure drop (voltage) across the segment ΔP_i is equal to product of flow rate (current) in the segment and the hydrodynamic resistance

$$\Delta P = Q_U R_U = Q_L R_L \tag{2}$$

Here R_U, R_L are the hydrodynamic resistances of upper and lower branches, respectively. The overall resistance of the branch is a sum of the static resistance due to the flow in rectangular channel ($R_{C,L}$), and resistance due to the droplets (n_L R_d), assuming n_L droplets in the lower branch

$$R_L = R_{C,L} + n_L R_d \tag{3}$$

Every droplet is assumed to increase the resistance of the channel linearly by R_d. The resistance of the rectangular channel is given by[38]

$$R_{C,L} = \frac{12\,\mu L}{h^3 w}\left[1 - \sum_n^{\infty} \frac{1}{n^5}\frac{192}{\pi^5}\frac{h}{w}\tan h\left(\frac{n\pi w}{2h}\right)\right]^{-1} \tag{4}$$

where h, w, and L are the height, width, and length of the lower branch respectively. μ represents the viscosity of the hexadecane oil and n is the series index which takes only odd values. The velocity of the droplets is proportional to the bulk flow,[39,40] and is given as follows

$$V_L = \frac{\beta}{S} Q_L \tag{5}$$

In the above equation V_L represents the velocity of droplets in the lower branch, β is a proportionality constant and S is the cross sectional area of the channel. At the junction, droplets are assumed to choose the branch with least resistance or maximum instantaneous flow rate. Similar equations are used to calculate the resistance and velocity of the upper branch. The model equations are solved as follows. Initially the flow rates in the branches are calculated using Eqs. 1–4. Based on the flow rates, the velocities of the droplets are updated using Eq. 5. These new velocities are used to obtain the positions of the droplets in the loop device. Positions and velocities are updated only when the droplet enters or exits the loop. This reduces the simulation time substantially. The exit times of the droplets from the model are compared with the experimental data by using R_d and β as free parameters. The best fit parameters are identified by comparing the experimental and simulated Poincaré maps. In Figure 3, the comparison between experimental data and the simulated data for the three-period and aperiodic dynamics are shown. For the explored cases, we observed that simulation results are in good agreement with the experimental dynamics. From here on we will use the model in lieu of the experimental system for simulation studies of the proposed feedback controller. Note that the same R_d and β values obtained from comparing experiments and model, are also used in the controller design (c.f. as shown in the "Model Predictive Control").

Description of Control Strategy

The main objective of this work is the development of a control algorithm for sorting and synchronizing droplets in microfluidic loop devices using active control. Conventional control algorithms such as proportional-integral-derivative (PID) are not suitable for nonlinear processes that exhibit multiple steady-states and chaos.[41] Instead, here, we implement a model predictive control (MPC) algorithm that uses the network model to regulate droplet behavior to achieve sort and synchronization. Two key principles are used in the proposed active MPC strategy for achieving these objectives. First, through valve actuation, the number of droplets in the upper and lower branches are made equal or differ by just one droplet at every time instant. Since the length of upper and lower branches in our loop device are nearly equal, this strategy ensures that the droplets alternate between the branches. Second, appropriate droplet velocity manipulations for synchronization are achieved through active resistance changes in the two arms of the loop. A possible online implementation of the MPC strategy is presented in Figure 1. Consider a train of alternate white and black droplets to enter the loop. These droplets are required to be sorted into the upper and lower channels and a pair of droplets exit the channel at the same time. At every sampling time images from the loop device are acquired using a high speed camera. These images can be processed to obtain current droplet

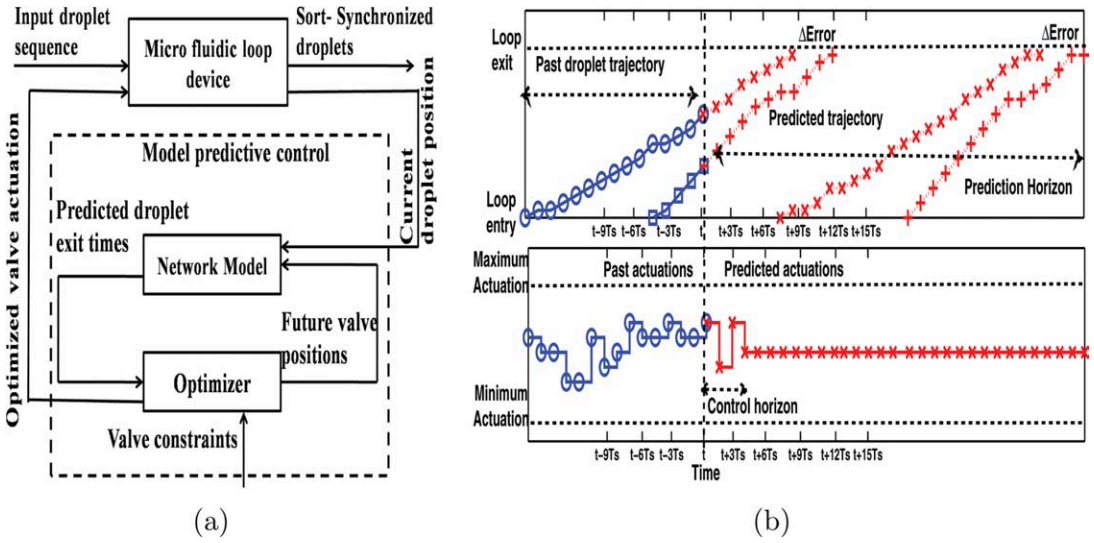

Figure 4. (a) Block diagram of MPC implementation on loop device (b) Illustration of prediction and control horizons in sort-synchronization framework of MPC.

[Color figure can be viewed in the online issue, which is available at wileyonlinelibrary.com.]

positions. These positions are the inputs to the MPC algorithm which calculates the optimum valve actuation required to synchronize the droplets. In the next section, the fundamentals of MPC are introduced and simulation studies incorporating the MPC algorithm are discussed.

Model Predictive Control

Model predictive control (MPC), also referred to as moving horizon control or receding horizon control has become an attractive feedback strategy for linear and nonlinear process control. Although MPC has been successfully implemented in other engineering applications[42,43] to our knowledge, this study is the first application of MPC in microfluidic devices. The main objective of MPC is to maintain outputs at their desired values, also termed as set points, through the actuation of manipulated variables. MPC possesses the following important attributes: (1) simplicity, (2) richness to solve a variety of control problems, and (3) constraints handling (equipment constraints, operational constraints).[44]

Description

There are two important components in a MPC. The first is the underlying model of the process that is used to predict the effect of the actuators (manipulated variables/elastomeric valve) on the variables of interest (controlled variables/droplet position). The second component is an optimizer that identifies values for the manipulated variables and ensures the error between the controlled variables and their target values are minimized. The control objectives in a microfluidic device are to sort and synchronize pairs of droplets. Sorting requires actuation whenever there is a droplet at the inlet junction. Synchronization requires a more continuous actuation to ensure that pairs of droplets exit at the same time. The controlled variable chosen for synchronization is the difference in the time exits between the leading droplets in the upper and lower branches. A target value of zero for this variable implies that synchronization has been achieved. The overall implementation of MPC is shown in Figure 4. From the microfluidic device, the position of the droplets are provided to the model predictive controller. The controller iteratively solves for optimum valve actuations required to sort-synchronize droplets using the network model as shown in the dotted box of Figure 4a. Two important tuning parameters dictate the final MPC performance. One is the prediction horizon, which is the time horizon into the future where the errors (between the predicted controlled variables and their target values, as represented in Figure 4b synchronization error) are minimized. Second is the control horizon, which determines the number of future actuations that are calculated at the current time instant. Figure 4b illustrates these parameters, droplet trajectories and the corresponding valve actuations as a function of time. The vertical dotted line in Figure 4b represents the current time instant and separates the past from the future. The trajectory of a droplet pair is predicted till it exits the device. This trajectory is shown in the top graph of Figure 4b. The time it takes for two droplet pairs to exit, based on the predicted trajectory is termed the prediction horizon. Hence the prediction horizon is a variable and changes with the position of droplet pair. This prediction horizon will be an integer multiple of the sampling time used for image capture. It is assumed that a certain prespecified number of valve actuations are performed at successive sampling times starting from the current time instant for synchronization. This is termed as control horizon, shown in the bottom graph of Figure 4b. Though several control moves are actually calculated only the first move is implemented and a new optimization problem is solved at the next time instant. This strategy would result in the use of the latest information available about the loop device in the valve actuation calculations at any given time. At every time instant one would ideally like to calculate the valve actuation for the whole prediction horizon; however, this would result in a large computational burden on the optimizer making online implementation difficult. In view of this, the prediction and control horizons are optimally chosen to achieve a balance between the computational burden and control accuracy. Increasing the control horizon will increase the computational burden while decreasing it will result in reduced control accuracy. The control horizon is always smaller in time length than the prediction horizon.[44] The optimizer takes into account the constraints on the hydrodynamic resistance imposed by the

valve and calculates the optimum valve actuation, which are implemented on the loop device. In the next section, the algorithmic details of the MPC approach are discussed.

Methodology

The MPC algorithm consists of four conceptual components for sort-synchronizing droplets.

Prediction. In this step, the future droplet positions are predicted based on the current positions. Let the current position of *i*th droplet in the lower branch of the loop, at a time instant "*t*", be $P_{i,L}(t)$. The positions of all the droplets at this time instant are given as inputs to the controller; the network model in the MPC predicts the future positions for a time of KT_s, where T_s (sampling time) is the prespecified time between two successive images analyzed by the controller and K is an integer. Here KT_s is defined as the prediction horizon. In the simulations the value of sampling time is calculated as follows

$$T_s = \max\left(5.5\,\text{ms},\ \frac{\tau}{20}\right) \tag{6}$$

In the above equation, τ is the mean residence time of the droplets, i.e. the mean difference in entry and exit time of the droplets. In general, the sampling time is chosen as a fraction of the time constant or settling time and the choice of $\tau/20$ is standard.[45] If the calculated sampling time is less than experimentally accessible sampling speed of about 5.5 ms[37] then 5.5 ms is chosen as the sampling time as shown in Eq. 6. The future positions of droplets in the lower branch are equal to the sum of current position of the droplets and the product of instantaneous velocity with sampling time, calculated as follows

$$\hat{P}_{i,\mathrm{L}}(t+KT_s|t) = P_{i,\mathrm{L}}(t) + \sum_{j=1}^{K} \hat{V}_{j,\mathrm{L}} T_s \tag{7}$$

where $\hat{P}_{i,\mathrm{L}}(t+KT_s|t)$ is the predicted position of the droplets in the lower branch given the positions at time *t*. The value of *K* in Eq. 7 is chosen just large enough so that two pairs of droplets exit the loop. As the loop structure is analogous to a parallel connection of resistances, the velocity in a branch is equal to the fractional resistance multiplied by the total flow rate. Therefore, the predicted velocity of the droplet $\hat{V}_{j,L}$ in Eq 7 at any time instant is calculated as follows

$$\hat{V}_{j,\mathrm{L}} = \frac{\beta}{S}\left[\frac{R_{j,\mathrm{U}}}{R_{j,\mathrm{L}} + R_{j,\mathrm{U}}}\right] Q_{\mathrm{I}} \tag{8}$$

The resistances of the branches customized for the external valve dynamics is sum of three components; channel resistance, droplet resistance and the fractional increase in resistance due to external valve, given as follows

$$\begin{aligned} R_{j,\mathrm{U}} &= R_{\mathrm{C,U}} + n_{j,\mathrm{U}} R_{\mathrm{d}} + \alpha_{j,\mathrm{U}} R_{\mathrm{C,U}} \\ \alpha_{j,\mathrm{U}} &= \alpha_{3,\mathrm{U}} \ \forall\ j > 3 \end{aligned} \tag{9}$$

$$\begin{aligned} R_{j,\mathrm{L}} &= R_{\mathrm{C,L}} + n_{j,\mathrm{L}} R_{\mathrm{d}} + \alpha_{j,\mathrm{L}} R_{\mathrm{C,L}} \\ \alpha_{j,\mathrm{L}} &= \alpha_{3,\mathrm{L}} \ \forall\ j > 3 \end{aligned} \tag{10}$$

The value of $R_{\mathrm{C,L}}$ is calculated using Eq. 4. $n_{j,U}$ and $n_{j,L}$ are the number of droplets in upper and lower branches respectively. $\alpha_{j,L}$ is the lower branch valve actuation parameter, which is to be estimated, and is constant after three steps as the control horizon in the simulations is chosen as three. Note that alpha equals zero corresponds to no actuation of the valve, and a nonzero value of alpha ($0 < \alpha < 1$) implies that the channel is being constricted due to valve actuation. Similar equations are used to predict the droplet positions in the upper branch.

Optimization for Synchronization. In this step, the optimal valve actuations required to sort-synchronize the droplets are calculated. Synchronization is achieved when two droplets exit the loop at the same time. The exit time of the droplets is defined as the time taken by the droplet to reach the end of the branch ,i.e., when the position of the droplet equals the channel length. The values of $T^i_{\mathrm{exit,L}}$ and $T^i_{\mathrm{exit,U}}$ time of droplet in upper and lower channel) are calculated as follows:

$$\begin{aligned} T^i_{\mathrm{exit,L}} &= t + K_1 T_s \ :\ \left\{ \begin{array}{c} \forall K \ \geq\ K_1\, \hat{P}_{i,\mathrm{L}}(t+KT_s|t) \ \geq\ L_{\mathrm{L}} \\ \forall K < K_1\, \hat{P}_{i,\mathrm{L}}(t+KT_s|t) < L_{\mathrm{L}} \end{array} \right\} \\ T^i_{\mathrm{exit,U}} &= t + K_2 T_s \ :\ \left\{ \begin{array}{c} \forall K \ \geq\ K_2\, \hat{P}_{i,\mathrm{U}}(t+KT_s|t) \ \geq\ L_{\mathrm{U}} \\ \forall K < K_2\, \hat{P}_{i,\mathrm{U}}(t+KT_s|t) < L_{\mathrm{U}} \end{array} \right\} \end{aligned} \tag{11}$$

L_{U} and L_{L} are the lengths of upper and lower branches, respectively. The time $(t + K_1T_s)$ at which the value of $\hat{P}_{i,\mathrm{L}}(t+KT_s|t)$ is equal to L_{L} is the exit time of that droplet. The optimum valve actuations for sort-synchronization are obtained by minimizing the objective function given by the following equation

$$\begin{aligned} \min_{\alpha_{(1,2,3),L},\alpha_{(1,2,3),U}} E &= \sum_{D=i}^{i+1} [T^D_{\mathrm{exit,L}} - T^D_{\mathrm{exit,U}}]^2 \\ 0 \ \leq\ \alpha_{1,\mathrm{L}}, \alpha_{1,\mathrm{U}} \ &\leq\ 0.6 \\ 0 \ \leq\ \alpha_{2,\mathrm{L}}, \alpha_{2,\mathrm{U}} \ &\leq\ 1 \\ 0 \ \leq\ \alpha_{3,\mathrm{L}}, \alpha_{3,\mathrm{U}} \ &\leq\ 1 \end{aligned} \tag{12}$$

E is sum of the squared errors of differences in exit times of *i*th and $(i + 1)$th pair of droplets, i.e, two from the upper branch and two from the lower branch. From our simulation studies we observed that the prediction horizon with less than two pairs of droplets make the control action oscillatory. On the other hand, choosing the prediction horizon to be more than two pairs of droplets would increase the computational complexity of the control calculations. Hence we used two pairs of droplets as a trade-off between good control and computational tractability. In our specific MPC implementation, we have set the control horizon to be equal to $3T_s$ as seen in Eq. 12, where the upper and lower limits on the three valve actuations are provided. We find this control horizon to be sufficient for our purposes. Also notice that while the first control move is constrained to be less than 60% (0.6)[37] in Eq. 12, the next two control moves are not constrained, (i.e., $\alpha = 1$). For computational reasons the optimizer assumes that three values of valve actuations are implemented to achieve synchronization. However, the valve actuations being implemented at every time instant results in considerably more than three actuations before a pair of synchronized droplets exit. To reflect this extra actuation, the bounds on two out of the three valve moves are relaxed (set to 100%, i.e., $\alpha = 1$ in our case). However, since the

first control move is actually implemented the bound for that is set to a realistically achievable value of 60%. We note that to optimize the objective function six α values need to be determined (c.f. Eq. 12). The simultaneous optimization is performed using Matlab optimization routine "fmincon".

Synchronization Actuation. As discussed before only the first values, i.e., $\alpha_{1,L}$ and $\alpha_{1,U}$, are implemented in the experiment even though three control moves are calculated.

Sorting Actuation. The previous steps ensure that a pair of droplets exit the loop due to synchronization. Therefore, the number of droplets in the upper and lower branches will be either equal or differ by one. Whenever a droplet enters the loop (we assume that this is detected just before the droplet enters the loop), the valves are set to the normal position, i.e., zero actuation. This ensures that every pair of droplets take the same decision as the first pair that entered the loop device. This results in sorting of the droplets. This control is achieved as an "interrupt" in the algorithm i.e. this step is implemented only when there is a droplet entry.

Results and Discussion

In this section the results obtained by implementing the proposed algorithm on the model explained in section are discussed. The results are presented in three subsections. Two of these deal with control results for the three period and aperiodic dynamics. The third subsection will explore the robustness of MPC control to fluctuations in the input feeding frequency of drops into the loop. In the first two cases, MPC has been implemented assuming the input droplets arrive at a constant input frequency. In the comparison plots shown in Figure 3, the scatter observed in the Poincaré map of the experimental data is due to the disturbances in the input flow rate (variations in the entry time of droplets). However, in the first two simulation case studies, these disturbances are not taken into account. Hence all the Poincaré maps that are shown in the results section will have well-defined clusters with no scatter due to input uncertainties. Further, a repeated sequence of droplets of alternating composition (e.g., BWBWBW…) is assumed at the entrance of the device. In all cases, we assume that valve actuation can potentially increase the hydrodynamic resistance of the branch from its base value to a maximum of 60%, i.e., $\alpha \leq 0.6$.

Three period dynamics

The first result that we show is for the case of three period behavior. The MPC algorithm, as discussed in the previous section, is implemented for this case. The actuations implemented on the system are the MPC calculated values rounded off to a precision of 0.1. This is to ensure that the precision required from the actual valve actuations are realizable in practice. The sorting of the droplets in the active and passive scenarios are shown in Figure 5a, which is a plot of droplet decisions with the droplet entry index. The droplets at the junction have two choices to make, either to go to the upper branch or lower branch. This plot shows the decision making of the droplets at the entrance to the bifurcation. The top graph of Figure 5a is with active control and the bottom graph is without active control. It is observed that without active control two droplets decide to choose the lower branch and one droplet chooses the upper branch and this pattern repeats. However, the droplets are sorted after implementation of MPC. The reason for failure in passive sorting is due to the entry of droplets in the loop before a pair of droplets exit. This situation results in alteration of droplet decisions. After the implementation of MPC, since two droplets exit the loop simultaneously due to synchronization, the incoming droplets encounter the same ratio of droplets in upper and lower branch at every time instant. This ensures sorting because of nearly symmetric loop device. As the decision of the droplets repeats after three steps in the uncontrolled case we observe a three cluster behavior in the Poincaré map (Figure 5b). After implementation of MPC, the loop dynamics has changed from three clusters to two clusters. This is because the droplets are constrained to make prespecified choices. It is also observed that the clusters are close to the axis. This is due to the decrease in difference between the droplet pair exit times, which is a measure of synchronization. As ΔT_{n+1} is plotted as a function of ΔT_n in a Poincaré map, perfectly synchronized pair of droplets at the exit will result in a data point each on the x and y axes. The magnitude of synchronization (zero being the best) is inferred from Figure 5c, which is a plot of difference in droplet pair exit times, normalized with mean difference in inlet time, as a function of droplet pair index. It can be seen from synchronization results shown in Figure 5c that the difference in the exit times of droplets is close to zero. This implies that all the droplet pairs are synchronized. The droplet trajectories, i.e., positions of droplets normalized with channel length, of four droplet pairs as a function of time are shown in Figure 5d. It is also observed from this figure that that the droplets are synchronized at the exit of the loop. This sort-synchronization is achieved with valve actuation within the bounds of 60 %. The valve actuations for this case are given in Figure 5e. In this figure, the fractional resistance changes in the upper and lower branches are plotted for each time instant. Figure 5f reports a plot between the actuation value and the ratio of number of actuations at that value to the total number of actuations. In this case, both the lower and upper branch valves have been actuated for 204 and 113 times, respectively. Due to this actuation a pair of 35 droplets were sort-synchronized in 3.3 s. In Figure 5e inset it is observed that the lower branch has zero actuation at regular intervals. As discussed before this is to achieve sorting of the droplets. The inset in the Figure 5e depicts a magnified plot of this "interrupt signal." These results demonstrate that the MPC-based feedback controller works extremely well for sorting and synchronizing droplets in the three period case.

Aperiodic dynamics

The second case we consider is that of aperiodic behavior. This is a very interesting case because active control strategy has to convert a system with chaotic dynamics and a large number of periods to a two period system. It can be seen from Figure 6a that passive sorting is completely aperiodic, i.e., the droplet decision making is chaotic as time progresses. However, MPC is able to sort the droplets into the two branches effectively. The Poincaré map of the system without control (Figure 6b) is characterized by several periods (more than 20). MPC converts the overall chaotic loop dynamics to two clusters in a Poincaré map. It is observed from the Poincaré map that these clusters also are very close to the axis which implies that the droplets have synchronized. The droplet synchronization dynamics are shown in Figure 6c. Compared to the uncontrolled case, the MPC approach results in remarkable synchronization of droplets

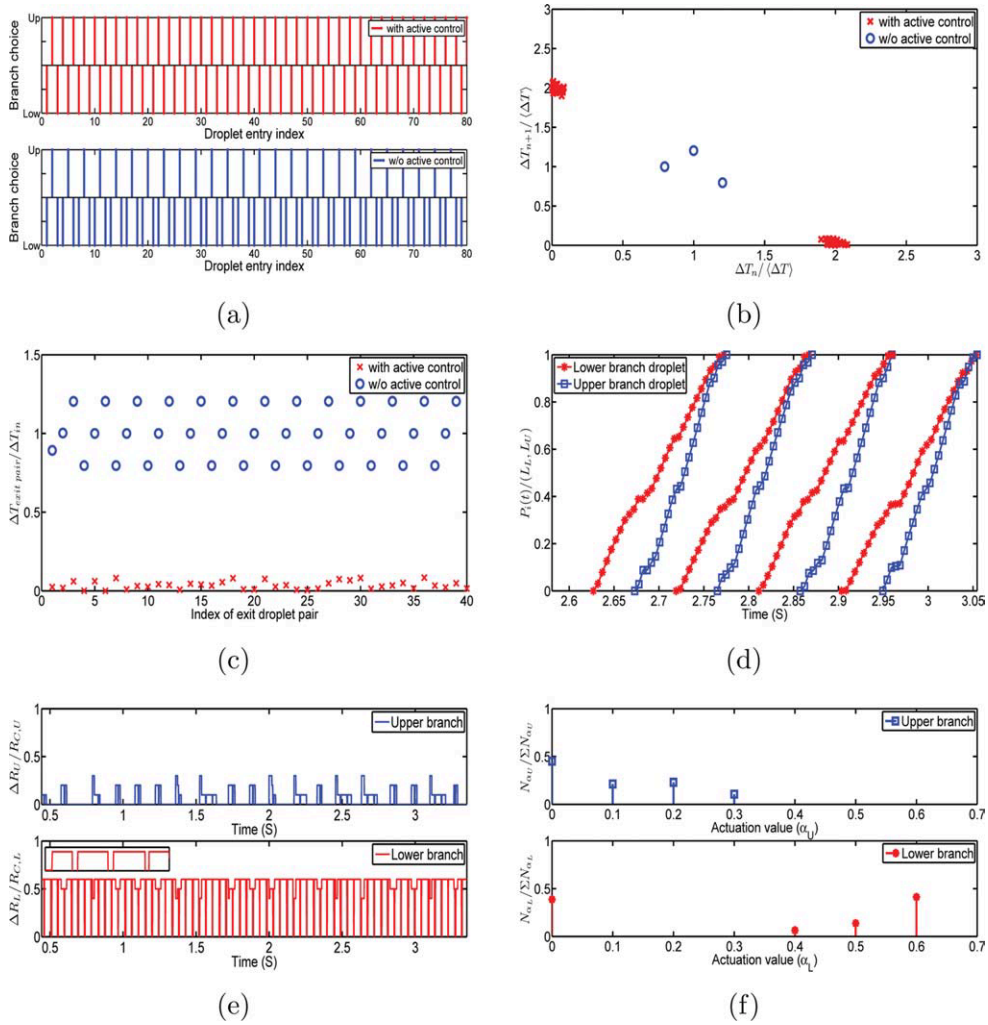

Figure 5. Model predictive control for three period case (a) Representation of sorting of droplets with and without actuation, (b) Behavior of Poincaré map with and without actuation in case of three period dynamics, (c) Representation of synchronization of droplet pairs with and without actuation, (d) Synchronized droplet trajectories of four droplet pairs with maximum achievable actuation set to 60% (e) Valve actuation required to sort-synchronize the droplets in lower and upper branches of the loop as a function of time.

The periodic dips in the actuation are shown in the inset. (f) Actuation frequency as a ratio of number of actuations at a particular value to the total number of actuations for synchronizing 35 pairs of droplets. [Color figure can be viewed in the online issue, which is available at wileyonlinelibrary.com.]

for this highly aperiodic system. The droplet trajectories as a function of time are shown in Figure 6d. As seen from this plot at any given time instant there are more than five droplets in the loop. Surprisingly, it is observed in this case that the lagging droplet overtakes the leading droplet before exiting the loop. This phenomenon is due to decrease in inlet flow rate and presence of more than five droplets in the loop that reduces the droplet velocities substantially. The valve actuations required to make the droplets sort and synchronize are represented in Figure 6e with the frequency of actuation in Figure 6f. In this case both the upper and lower valves have been actuated for 162 and 165 times, respectively to sort-synchronize 35 pairs of droplets over a time span of 4.2 s. As before, sorting requires the valve to move to zero and this is shown in the inset of Figure 6e. Similar to the three period case, the upper branch valve is also actuated. This is because the lagging droplet overtakes the leading droplet which necessitates actuation in the upper branch to slow down the droplet. One might intuitively expect more vigorous actuation for an aperiodic case. Surprisingly, the lower branch actuation stays substantially at 50% rather than 60%, which was observed in the three period case. This is because the velocities of the droplets are low (due to high resistance as a result of low flow rate and more droplets in the device) and hence there is more actuation time, which results in less aggressive actuation. However, nuanced actuations of the upper and lower branches as in the three period case are required in the aperiodic case also.

Robustness of MPC to input flow fluctuations

In this simulation experiment, we test the robustness of MPC to fluctuations in the inlet times which are measured experimentally. The inlet time fluctuations are most likely the result of disturbances in the input flow.[46] To reflect this, we introduce a 5% random disturbance in the inlet flow in the prototypical model. This disturbance changes the

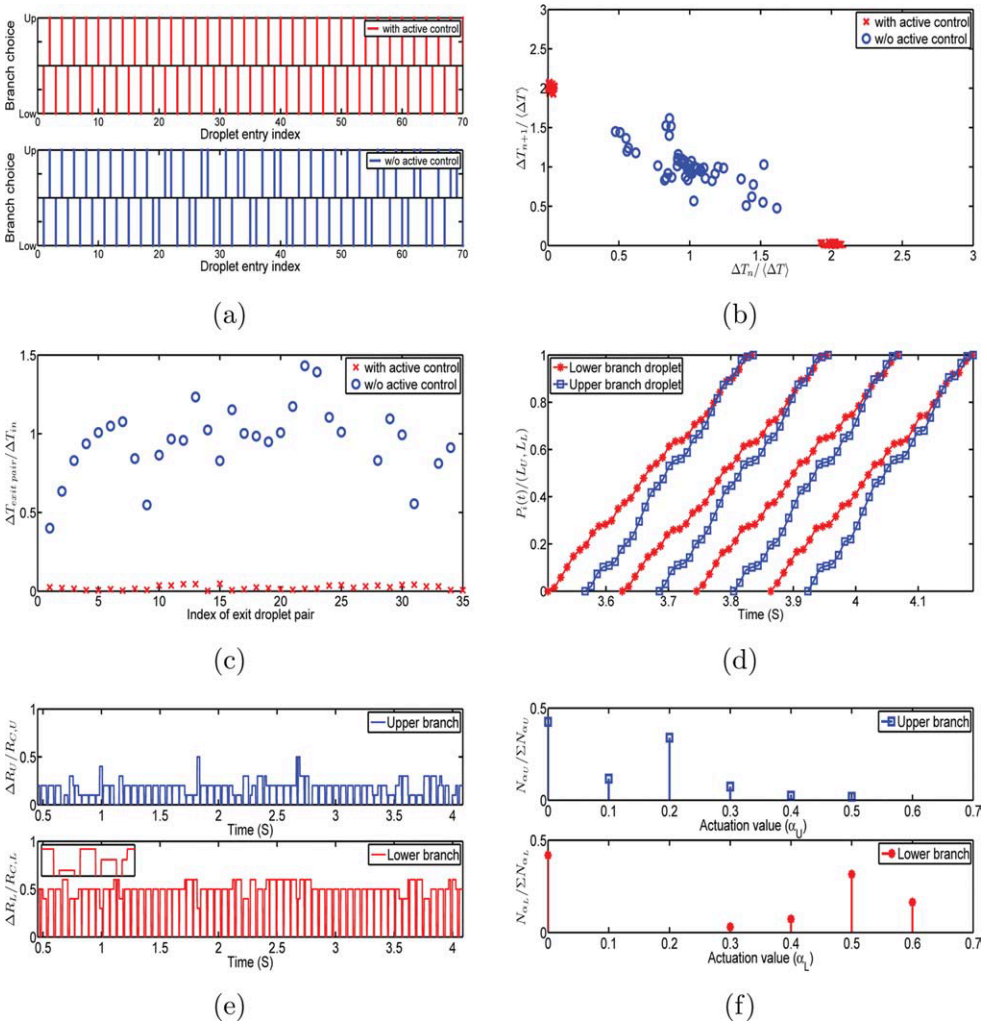

Figure 6. Model predictive control for aperiodic case (a) Representation of sorting of droplets with and without actuation, (b) Behavior of Poincaré map with and without actuation in case of aperiodic dynamics, (c) Representation of synchronization of droplet pairs with and without actuation, (d) Synchronized droplet trajectories of four droplet pairs with maximum achievable actuation set to 60%, observe the overtaking of lagging droplet in the inset, (e) Valve actuation required to sort-synchronize the droplets in lower and upper branches of the loop as a function of time.

The periodic dips in the actuation are seen in the inset. Interestingly in this case the upper branch also gets actuated consistently (f) Actuation frequency as a ratio of number of actuations at a particular value to the total number of actuations for synchronizing 35 pairs of droplets. [Color figure can be viewed in the online issue, which is available at wileyonlinelibrary.com.]

residence time of the droplets as the overall flow changes. Experimental inlet time intervals of the droplets in the three period case as shown in the inset of Figure 7b are used along with random flow fluctuations in the prototypical model. However, the model for prediction in the MPC has no knowledge of this and hence constant flow and average inlet time interval as shown in the inset of Figure 7b are used. It can be seen from Figure 7a that even with input fluctuations, perfect sorting has been achieved. Unlike the previous case where disturbance was not considered, this case required more rigorous actuation to achieve synchronization (Figure 7e). With this actuation, satisfactory synchronization is achieved as shown in Figures 7c, d. This is despite the substantial variation in the input time intervals towards the end of this simulation. The actuation in the upper branch has increased to the maximum towards the end of the simulation; this is because of the dramatic offset in the inlet time intervals (seen in the inset of Figure 7b). Figure 7f shows the frequency of upper and lower branch actuations. Hence without a priori knowledge of the disturbance, MPC could tune itself for the fluctuations. In contrast to the no disturbance case, in this simulation, even the upper branch has been actuated to its maximum value.

Feasibility of Implementing Active Control

Our results in this paper demonstrate that the model-based feedback controller is able to achieve sort-synchronization tasks in a loop device. In our simulations, the sampling time is taken as 6.3 ms and 15.1 ms for three period and aperiodic cases respectively based on Eq. 6. The maximum possible actuation is set to 60% resistance change. Prior studies have shown that the minimal response time of the elastomeric valves is about 5 ms, and they can increase the channel resistance to as high as 68%,[37] suggesting that the

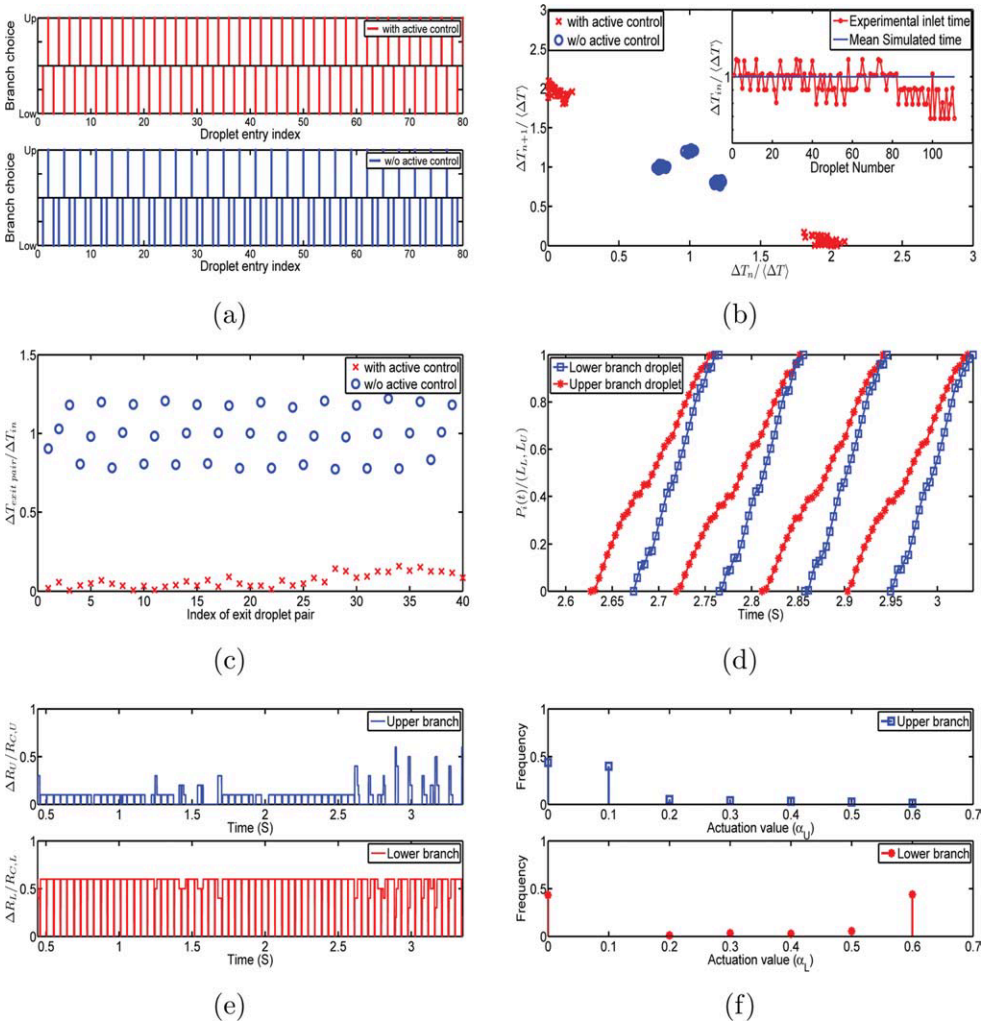

Figure 7. Simulation results with experimental inlet times and random flow fluctuations (a) Representation of sorting of droplets with and without actuation, (b) Behavior of Poincaré map with and without actuation in case of three period dynamics, (c) Representation of synchronization of droplet pairs with and without actuation, (d) Synchronized droplet trajectories of four droplet pairs with maximum achievable actuation set to 60%, observe the proper synchronization of lagging droplet, (e) Valve actuation required to sort-synchronize the droplets in lower and upper branches of the loop as a function of time, (f) Actuation frequency as a ratio of number of actuations at a particular value to the total number of actuations for synchronizing 40 pairs of droplets.

Plot of variation in the experimental inlet times is shown in the inset of figure (b). [Color figure can be viewed in the online issue, which is available at wileyonlinelibrary.com.]

parameter values chosen in the simulation are accessible by experiments. For online implementation of this approach, concerns related to actuator dynamics and computational complexity of MPC calculations need to be addressed. For the loop structure, the droplets exit at around 40 milliseconds (ms) time intervals. The time required for one actuator move is about 10 ms. If the sampling time is chosen to be 10 ms, then about four actuator moves can be made before the exit of droplet. This, we believe, should provide enough actuation for the control of individual droplet exit times. The physical model took about 1s for the calculation of the trajectory of 1000 droplets on a standard PC. This would imply that roughly about 1 ms would be required to calculate the trajectory of a single droplet. This could be improved five-to-ten fold using a sophisticated dedicated computer. Further, in the 1000 droplets simulation, most of the time is spent on data structures to store the results for all the 1000 droplets. Since only 5–10 droplets will be present in the loop at a time, each MPC calculation has to deal with a small number of droplets. Hence the data storage related time will reduce drastically. In summary, we expect that 1000 function evaluations can be performed within 10 ms. As a result, the use of standard gradient-based approaches for online control calculations might be feasible; however, a direct approach such as the Nelder–Mead simplex search[47] that handles constraints might be more computationally appropriate for this problem. Another approach to mitigate online computational issues is to investigate if satisfactory online control results could be achieved by directly implementing the actuations that are calculated off-line using the proposed MPC approach.

Conclusions

In this work, we propose the idea of active resistance modulation for controlling the position and timing of droplets in fludic networks. To this end, we investigate this concept in a simple microfluidic loop. A key finding from this work is that resistance control can help achieve precise sorting and synchronization of droplets at the outlet of the device even in cases where uncontrolled dynamics are chaotic. We believe that this controllability result has never been demonstrated before. While this is a first step in this area, controllability in more complex networks might be challenging. We anticipate that a suitable choice of resistance control in a subset of branches may extend the applicability of the MPC strategy to more intricate networks and needs to be explored in the future.

On the practical side, the proposed control algorithm needs to be implemented on the experimental loop device using elastomeric valves. This will help uncover if there are real impediments to the proposed approach such as, breakage of droplets due to the elastomeric valve actuation. Such an experimental study will truly verify the promise of model based feedback control in droplet-based microfluidic devices.

Acknowledgments

S.A.V. acknowledges support from NSF CBET 0932796 and participation by Timothy Corini in the study through a NSF REU program (MANDE Grant No: 0648761). R.R. acknowledges NSF CBET 0553992 for some of his time and start-up funds from Texas Tech University for his students (Jeevan Maddala and Babji Srinivasan) support.

Literature Cited

1. Zheng B, Tice JD, Ismagilov RF. Formation of droplets of alternating composition in microfluidic channels and applications to indexing of concentrations in droplet based assays. *Anal Chem*. 2004;76:4977–4982.
2. Haeberle S, Zengerle R III. Microfluidic platforms for lab-on-chip applications. *Lab Chip*. 2007;7:1094–1110.
3. Brouzes E, Medkova M, Savenelli N, Marran D, Twardowski M, Hutchison JB, Rothberg JM, Link DR, Perrimon N, Samuels ML. Droplet microfluidic technology for single-cell high throughput screening. *PNAS*. 2009;106:14195–14200.
4. Song H, Chen DL, Ismagilov RF. Reactions in droplets in microfluidic channels. *Angew Chem Int Ed*. 2006;45:7336–7356.
5. Fernandez-Nieves A, Cristobal G, Garces-Chavez V, Spalding GC, Dholakia K, Weitz D. Optically anisotropic colloids of controllable shape. *Adv Mater*, 2005;17:680–684.
6. Xu S, Nie Z, Seo M, Lewis PC, Kumacheva E, Stone HA, Garstecki P, Weibel DB, Gitlin I, Whitesides GM. Generation of monodisperse particles by using microfluidics: control over size, shape, and composition. *Angew Chem Int Ed*. 2005;117:734–738.
7. Nie Z, Xu S, Seo M, Lewis PC, Kumacheva E. Polymer particles with various shapes and morphologies produced in continuous microfluidic reactors. *J Am Chem Soc*. 2005;127:8058–8063.
8. Huebner A, Srisa-Art M, Holt D, Abell C, Hollfelder F, deMello AJ, Edel JB. Quantitative detection of protein expression in single cells using droplet micrfluidics. *Chem Commun*. 2007;12:1218–1220.
9. Cristobal G, Benoit JP, Jaonicot M, Ajdari A. Microfluidic bypass for efficient passive regulation of droplet traffic at a junction. *Applied Physics Letters*. 2006;89:034104–1–034104–3.
10. Prakash M, Gershenfeld N. Microfluidic bubble logic. *Science*, 2007;315:832–835.
11. Bremond N, Thiam AR, Bibette J. Decompressing emulsion droplets favors coalescence. *Phys Rev Lett*. 2008;100:024501–1–024501–4.
12. Niu X, Gulati S, Edel JB, deMello AJ. Pillar-induced droplet merging in microfluidic circuits. *Lab Chip*. 2008;8:1837–1841.
13. Hatakeyama T, Chen DL, Ismagilov RF. Microgram-scale testing of reaction conditions in solution using nanoliter plugs in microfluidics with detection by MALDI-MS. *J Am Chem Soc*. 2006;128:2518–2519.
14. Shim J, Cristobal G, Link DR, Thorsen T, Jia Y, Piattelli K, Fraden S. Control and measurement of the phase behavior of aqueous solutions using microfluidics. *J Am Chem Soc*. 2007;129:8825–8835.
15. Qin J, Ye N, Lin B. Droplet-based microfluidic system for individual caenorhabditis elegans assay. *Lab Chip*. 2008;8:1432–1435.
16. Boukellal H, Selimovic S, Jia Y, Cristobal G, Fraden S. Simple robust storage of drops and fluids in a microfluidic device. *Lab Chip*. 2008;9:331–338.
17. Philippe L, Aurore C, Jean-Baptiste S. Microfluidic droplet method for nucleation kinetics measurements. *Langmuir*. 2009;25:1836–1841.
18. Bithi SS, Vanapalli SA. Behavior of a train of droplets in a fluidic network with hydrodynamic traps. *Biomicrofluidics*. 2010;4:044110–1–044110–10.
19. Tan YC, Fisher JS, Lee AI, Cristini V, Phillip A. Design of microfluidic channel geometries for the control of droplet volume, chemical concentration, and sorting. *Lab Chip*. 2004;4:292–298.
20. Christopher GF, Bergstein J, End NB, Poon M, Nguyen C, Anna SL. Coalscence and splitting of confined droplets at microfluidic junctions. *Lab Chip*. 2009;9:1102–1109.
21. Jin BJ, Kim YW, Lee Y, Yoo JY. Droplet merging in a straight microchannel using droplet size or viscosity difference. *J Micromech Microeng*. 2010;20:035003–1–035003–3.
22. Cybulski O, Garstecki P. Dynamic memory in a microfluidic system of droplets traveling through a simple network of microchannels. *Lab Chip*. 2009;10:484–493.
23. Fuerstman MJ, Garstecki P, Whitesides GM. Coding/decoding and reversibility of droplet trains in microfluidic networks. *Science*. 2007;315:828–832.
24. Schindler M, Ajdari A. Droplet traffic microfluidic networks: A simple model for understanding and designing. *Phys Rev Lett*. 2008;100:044501–1–044501–4.
25. Smith BJ, Gaver DP III. Agent-based simulations of complex droplet pattern formation in a two-branch microfluidic network. *Lab Chip*. 2010;10:303–312.
26. Engl W, Roche M, Colin A, Panizza P, Ajdari A. Droplet traffic at a simple junction at low capillary numbers. *Phys Rev Lett*. 2005;95:208304–1–208304–3.
27. Belloul M, Engl W, Colin A, Panizza P, Ajdari A. Competition between local collisions and collective hydrodynamic feedback controls traffic flows in microfluidic networks. *Phys Rev Lett*. 2009;102:194502–1–194502–3.
28. Jousse F, Farr R, Link DR, Fuerstman MJ, Garstecki P. Bifurcation of droplet flows within capillaries. *Phys Rev E*. 2006;74:036311–1–036311–6.
29. Ahn K, Kerbage C, Hunt TP, Westervelt RM, Link DR, Weitz DA. Dielectrophoretic manipulation of drops for high-speed microfluidic sorting devices. *Appl Phys Lett*. 2006a;88:0241 04–1–024104–3.
30. Ahn K, Agresti J, Chong H, Marquez M, Weitz DA. Electrocoalescence of drops synchronized by size-dependent flow in micrfluidic channels. *Appl Phys Lett*. 2006b;88:264105–1–264105–3.
31. Niu X, Zhang M, Peng S, Wen W, Sheng P. Real-time detection, control and sorting of microfluidic droplets. *BioMicrofluidics*. 2007;1:044101–1–044101–12.
32. Link DR, Grasland-Mongrain E, Duri A, Sarrazin F, Cheng Z, Cristobal G, Marquez M, Weitz DA. Electric control of droplets in microfluidic devices. *Angew Chem Int Ed*. 2006;45:2256–2560.
33. Wei W, Chun Y, YingShuai L, Ming LC. On-demand droplet release for droplet-based microfluidic system. *Lab Chip*. 2010;10:559–562.
34. Wei W, Chun Y, Ming LC. On-demand microfluidic droplet trapping and fusion for on-chip static droplet assays. *Lab Chip*. 2009;9:1504–1506.
35. Bhattacharjee B, Najjaran H. Droplet position control in digital microfluidic systems. *Biomed Microdevices*. 2010;12:115–124.
36. Abate AR, Agresti JJ, Weitz DA. Microfluidic sorting with high-speed single layer membrane valves. *Appl Phys Lett* 2010;96:203509–1–203509–3.
37. Abate AR, Weitz DA. Single-layer membrane valves for elastomeric microfluidic devices. *Appl Phys Lett*. 2008;92:243509–1–243509–3.
38. Bruus H. *Theoretical Microfluidics*. 1st ed.; New York: Oxford University Press, 2008.
39. Vanapalli SA, Banpurkar AG, van den Ende D, Duits MHG, Mugele F. Hydrodynamic resistance of single confined moving drops in rectangular microchannels. *Lab Chip*. 2009;9:982–990.

40. Labrot V, Schindler M, Guillot P, Colin A, Joanicot M. Extracting the hydrodynamic resistance of droplets from their behavior in microchannel networks. *BioMicrofluidics.* 2009;3:012804–1–012804–16.
41. Wayne BB. Nonlinear control of chemical processes: a review. *Indu Eng Chem Res*. 1991;30:1391–1413.
42. Morari M, Lee JH. Model predictive control: past, present and future, computers & chemical engineering. *Comput Chem Eng*. 1999;23:667–682.
43. Qin SJ, Badgwell TA. A survey of industrial model predictive control technology. *Control Eng Practice*. 2003;11:733–764.
44. Ogunnaike BA, Ray WH. *Process Dynamics, Modeling, and Control*. 1 ed.; New York: Oxford University Press, 1994.
45. Srinivasan R, Rengaswamy R. Use of inverse response sequence (IRS) for identification in chemical process systems. *I EC Res*. 1999;38:3420–3429.
46. Korczyk PM, Cybulski O, Makulska S, Garstecki P. Effects of unsteadiness of the rates of flow on the dynamics of formation of droplets in microfluidic systems. *Lab Chip*. 2011;11:173–175.
47. Nelder JA, Mead R. A simplex method for function minimization. *Comput J*. 1965;7:308–313.

Manuscript received Oct. 28, 2010, revision received Mar. 11, 2011, and final revision received Jul. 20, 2011.